Digest Journal of Nanomaterials and Biostructures Vol. 19, No. 3, July -September 2024, p. 1087 - 1093

Hydrothermal synthesis of $La_{0.5}Sr_{0.5}MnO_3$ nanostructures for enhanced CO oxidation

S. Priyatharshni[a,*], P. Sivakumar[b,*], N. Prabhu[a], C. Karthikraj[a], M. Gowtham[c]
[a]*R&D Laboratory, Department of Physics, Excel Engineering College (Autonomous), Namakkal – 637 303, Tamil Nadu, India*
[b]*R&D Laboratory, Department of Chemistry, Excel Engineering College (Autonomous), Namakkal – 637 303, Tamil Nadu, India*
[c]*Department of Aeronautical Engineering, Excel Engineering College (Autonomous), Namakkal – 637 303, Tamil Nadu, India*

This study focuses on the synthesis and characterization of $La_{0.5}Sr_{0.5}MnO_3$ (LSMO) perovskite nanostructures via the hydrothermal method and their catalytic performance evaluation in CO oxidation. Structural analysis using techniques like XRD, FE-SEM, FTIR, and Raman spectroscopy analysis verified the development of LSMO nanostructures exhibiting a rhombohedral phase configuration. The catalytic activity of the annealed LSMO nanostructures was assessed, demonstrating significant CO conversion efficiency attributed to structural modifications enhancing catalytic performance. These findings highlight the potential of LSMO perovskite nanostructures as efficient catalysts for CO oxidation.

(Received April 30, 2024; Accepted July 16, 2024)

Keywords: Perovskite-type oxide, Nanostructure synthesis, Catalytic oxidation, CO oxidation, Hydrothermal method, Structural characterization

1. Introduction

Carbon monoxide (CO) poses a significant threat to life due to its toxic nature, necessitating effective strategies for its oxidation to mitigate atmospheric pollution. Oxides of Perovskite-type exhibit significant interest due to their catalytic activity in oxidizing CO. These oxides exhibit a distinctive ABO_3 crystal structure, where cations with large ionic radii occupy A-sites and B-sites within the cubic closest packing of oxygen atoms. The structural integrity of perovskites, crucial for catalytic activity, is influenced by the tolerance factor, which ideally approaches unity under specific temperature conditions, resulting in an ideal crystal structure. Nevertheless, variations from this ideal configuration, including orthorhombic, rhombohedral, tetragonal, monoclinic, and triclinic symmetries, are noted under different environmental circumstances [1-3]. Nonstoichiometry in perovskites can arise from deficiencies in cations (A or B sites), as well as anion deficiencies or excesses.

Lanthanum-transition metal-based perovskites, introduced into catalysis around three decades ago [4,5], have emerged as promising candidates, with $La_{0.5}Sr_{0.5}MnO_3$ (LSMO) attracting particular interest due to its robust catalytic activity in CO oxidation. The stable perovskite structure allows for partial substitutions of La^{3+} or Mn^{3+} with foreign cations of different sizes and shell configurations, enhancing structural properties. For instance, substituting La^{3+} with Sr^{2+}, Ca^{2+}, Pb^{2+}, or Ba^{2+} promotes oxidation of Mn^{3+} to Mn^{4+}, creating ionic vacancies crucial for maintaining electroneutrality and catalytic performance [6-8].

Catalytic combustion stands as a crucial technique in addressing air pollution stemming from volatile organic compounds (VOCs), providing an effective means of decreasing emissions such as NO_x, CO, and unburned hydrocarbons [9-12]. LSMO perovskites, owing to their inherent stability and tailored properties, exhibit remarkable catalytic activity during CO oxidation [14-15]. The hydrothermal method stands out for preparing LSMO nanostructures, providing advantages

* Corresponding authors: svkmrplnsm@gmail.com
https://doi.org/10.15251/DJNB.2024.193.1087

such as high purity, controlled morphology, and unique particle size distributions critical for catalytic applications [16-18].

2. Laboratory procedure

2.1. Chemical substances and reagents

Every chemical employed within this investigation were of analytical reagent grade and utilized without additional purification. Dopamine, ascorbic acid, lanthanum nitrate ($LaNO_3$), strontium nitrate ($SrNO_3$), manganese nitrate ($MnNO_3$), citric acid ($C_6H_8O_7$), and potassium hydroxide (KOH) were procured from Himedia, India. Ethylene glycol (EG) was obtained from SD-Fine Chem. Ltd., India. Deionized water was used exclusively for preparing all solutions.

2.2. Instruments

The integrity of the phase and crystal structure of the synthesized nanostructures were analyzed using a powder X-ray diffractometer (XRD) equipped with Copper K-alpha radiation (wavelength=1.5417 angstroms) operating at 50 kilovolts (kV) and 300 milliamperes (mA). Fourier transform infrared (FT-IR) spectroscopy was employed for analyzing stretching and bending modes, utilizing a BRUKER Tensor-27 instrument. Morphology and composition studies were conducted using field emission scanning electron microscopy (FE-SEM) using a Quanta-250 FEG instrument at an acceleration voltage of 30 kilovolts (kV), along with X-ray energy dispersive spectroscopy (EDS). Chemical structure analysis was performed using Raman spectroscopy with Horiba LabRAM HR probes.

2.3. Production of LSMO nanostructures

The LSMO nanostructures underwent synthesis via the hydrothermal technique. Stoichiometric quantities of Lanthanum (III), strontium (II), and manganese (II) nitrates were utilized as initial materials, dissolved in deionized water to create a 0.5 M solution. Initially, separate solutions of La, Sr, and Mn nitrates, along with Cetrimide, were prepared in distilled water and agitated. The catalyst preparation occurred under basic conditions, where the aforementioned solutions were amalgamated and potassium hydroxide (KOH) was introduced to act as an oxidizing agent, maintaining the solution's pH at 12. Ethylene glycol was subsequently added, followed by stirring the resulting solution for a specified duration before transferring it into a Teflon vessel. The vessel was then subjected to an oven environment maintaining a temperature of 200 °C for 12 hours. Post-hydrothermal treatment, the mixture underwent washing with distilled water, subsequently dried at 100 °C for overnight. Finally, the substance underwent grinding using a mortar and pestle to enhance precursor homogeneity. The schematic illustration depicting the hydrothermal synthesis of LSMO nanostructures for CO oxidation is shown in Scheme 1.

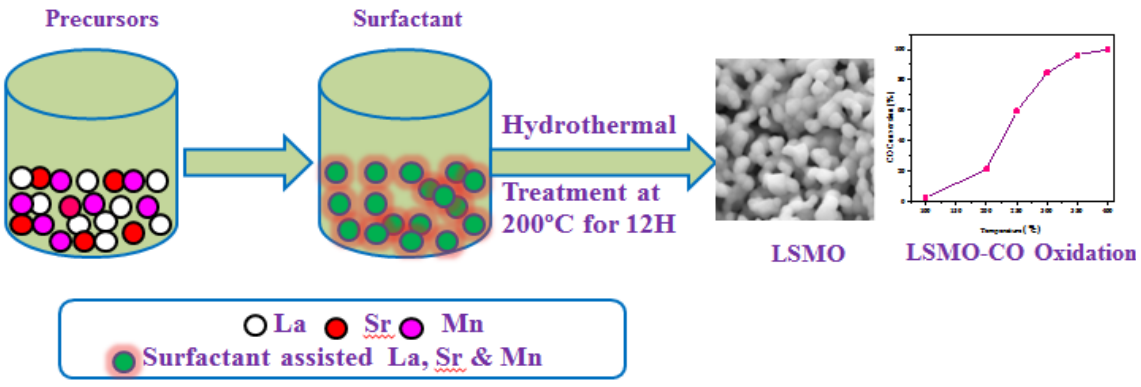

Scheme 1. Schematic illustration for the hydrothermal synthesis of LSMO nanostructures for CO oxidation.

2.4. Measuring catalytic activity

Catalytic activity was evaluated by means of fixed-bed quartz microreactor with an inner diameter of 5mm. To mitigate the risk of localized overheating, the substance, maintained at a 40-60 mesh size, was mixed with 0.25 g of quartz sands. Before conducting the tests, each sample was exposed to air (30 mL/min) was passed through the samples at 400°C for 0.5 hours, followed by cooling to the desired temperature. CO oxidation was performed using a reactant gas mixture consisting of 1% CO, 20% O_2, and N_2 as the remainder, was directed through the sample bed. The flow rate was around 10,000 mL/(g•h). Starting materials and resulting compounds were monitored in real-time using a gas chromatograph fitted with a thermal conductivity detector featuring a 13X column.

3. Findings and analysis

3.1. FE-SEM morphology examination and elemental analysis

FE-SEM images (Fig. 1a-d) depict surface morphologies of as-prepared and annealed LSMO nanostructures, highlighting changes in particle size and morphology with varying annealing temperatures.

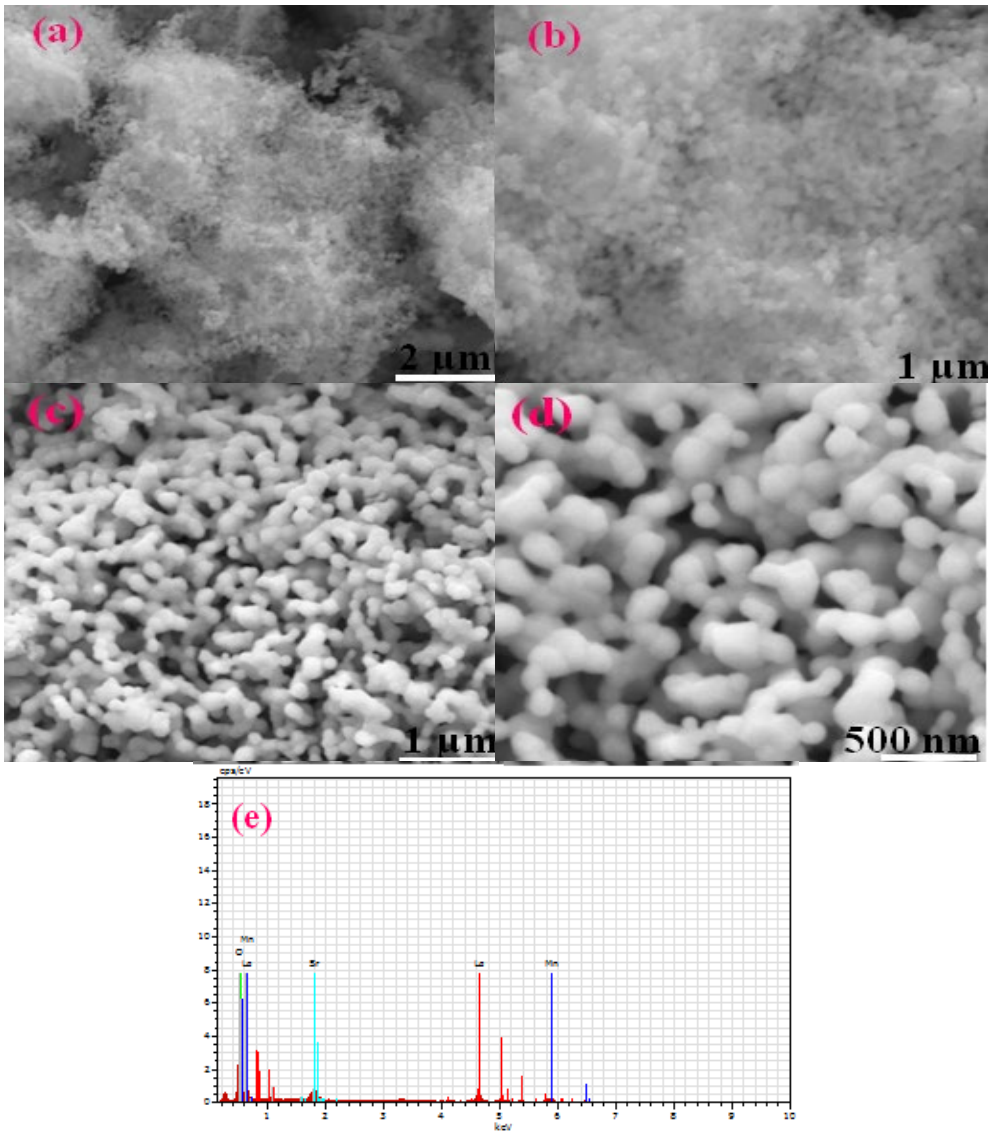

Fig. 1. FE-SEM image of LSMO nanostructures for (a) small and (b) large scale magnification before annealing; (c) small and (d) large scale magnification after annealing; (e) EDS spectra of annealed sample.

The as-prepared samples exhibited agglomerated particles with irregular shapes, while annealed samples at 900 °C for 3 hours displayed a porous network structure. The EDS spectrum confirmed the elemental composition of the nanoparticles, verifying their purity [19-21].

3.2. X-ray diffraction analysis

The XRD pattern depicted in Figure 2 (a, b) illustrates the as-prepared and annealed LSMO nanostructures synthesized via the hydrothermal method. Various factors influence the crystalline phase formation under hydrothermal treatment, including pH, temperature, and source materials. In our synthesis, the pH exceeded 7, and the temperature was kept at 200 °C, with the addition of KOH to ensure proper alkalinity. The introduction of KOH plays a crucial role in ion dissociation, leading to a color change to brown during its addition. The as-prepared sample exhibited amorphous behavior without any peaks, necessitating a calcination process to eliminate residual water and volatile components, thereby enhancing the sample's crystalline structure. Upon annealing at 900 °C for 3 hours, sharp peaks appeared, indicating a transition from amorphous to crystalline behavior. Substituting divalent Sr^{2+} for trivalent La^{3+} in the $LaMnO_3$ perovskite induced the formation of Mn^{4+} ions, creating cation vacancies. The XRD peaks post-annealing indicated well-shaped crystal growth with significantly increased intensity compared to the as-prepared sample. Intense peaks corresponding to (012), (110), (202), (024), (122), (214), (220), and (134) indices were observed, consistent with a crystalline rhombohedral phase structure, closely matching standard JCPDS #89-8094. The average crystallite size, estimated from the (110) peak using Scherrer's formula, was found to be 13 nm.

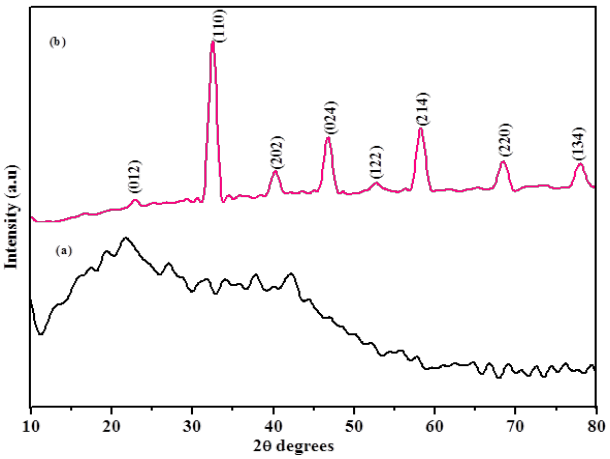

Fig. 2. XRD pattern of LSMO nanoparticles for (a) as prepared and (b) annealed nanostructures.

3.3. Fourier transform infrared spectroscopic analysis

FT-IR spectra (Figure 3 a, b) of as-prepared and annealed LSMO nanostructures were examined with the range of 400-4000 cm^{-1}. These spectra offer insights into the functional groups and chemical bonding of nanostructured materials. The absorbance peak at 600 cm^{-1} corresponds to the metal-oxygen bond stretching mode within the perovskite structure, confirming LSMO nanoparticle formation. Other observed bands at specific wavenumbers indicate various vibrations related to metal-oxygen and nitrogen-oxygen bonds, as well as functional groups from the synthesis process, such as CTAB and ethylene glycol. The presence of these bands confirms the successful formation of LSMO nanostructures and associated functional groups [22].

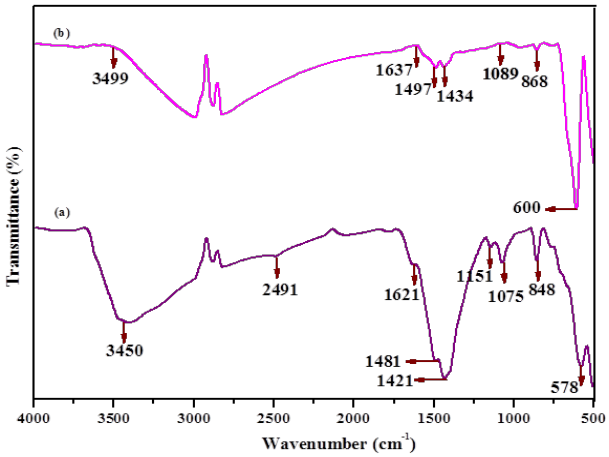

Fig. 3. FTIR spectroscopic analysis of LSMO nanoparticles for (a) as prepared and (b) annealed samples.

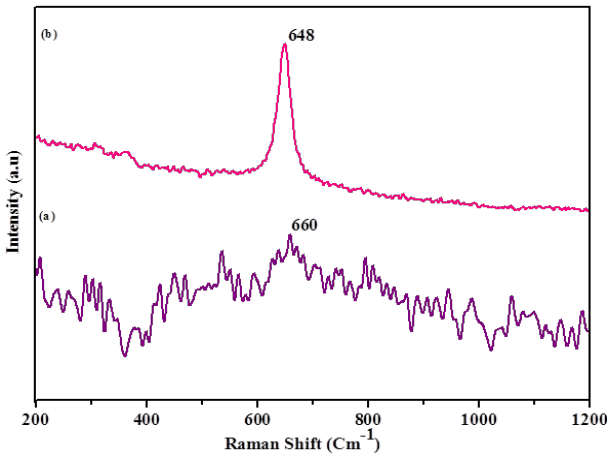

Fig. 4. Raman spectra of LSMO nanostructures for (a) as prepared and (b) annealed samples.

3.4. Raman spectroscopic analysis

Raman spectra (Figure 3 a, b) of as-prepared and annealed LSMO nanostructures reveal characteristic vibrational modes indicative of structural changes. The observed peaks at specific wavenumbers correspond to vibrational modes associated with Mn-O stretching vibrations of MnO_6 units, reflective of LSMO nanostructures characteristics. Changes in peak intensities and linewidths provide insights into structural alterations induced by annealing, such as the John-Teller effect and rhombohedral symmetry [23].

3.5. Catalytic activity profile

The catalytic activity profile (Figure 5) of annealed LSMO nanostructures for CO oxidation demonstrates their effectiveness at lower temperatures. Structural deviations, cationic vacancies, and surface composition changes play crucial roles in enhancing catalytic activity. The annealed samples exhibited a porous network structure, contributing to higher catalytic activity, attributed to increased active sites and surface oxygen vacancies facilitating CO oxidation. These results highlight the importance of structural control and surface modifications in tuning catalytic performance [24-26].

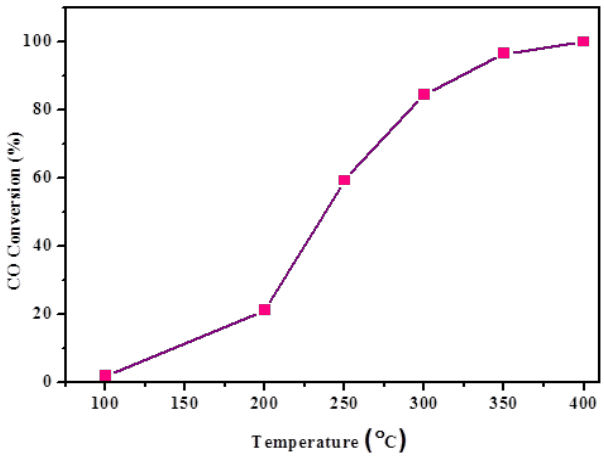

Fig. 5. Activity profile for the oxidation of CO for annealed LSMO nanostructures.

4. Conclusion

The synthesis of LSMO nanostructures via the hydrothermal method resulted in crystalline rhombohedral phase structures having an average crystallite size of 13 nm post-annealing at 900°C. Structural characterization using XRD, FTIR, and Raman spectroscopy confirmed the formation of LSMO nanostructures, revealing metal-oxygen bond vibrations and structural alterations due to cation substitutions. FE-SEM analysis showed a transition from agglomerated particles to a porous network structure, enhancing catalytic activity.

Catalytic activity measurements demonstrated significant CO conversion efficiency, with 10% conversion achieved at 158°C and 50% conversion at 230°C. The enhanced catalytic behavior was attributed to increased active sites, surface composition changes promoting oxygen vacancy formation, and Mn-rich terminated perovskite surface facilitating CO interaction.

These findings underscore the potential of LSMO perovskite nanostructures as efficient catalysts for CO oxidation, highlighting the importance of structural control and surface modifications in tuning catalytic performance.

Acknowledgements

The authors extend their appreciation to all individuals who contributed to this study.

References

[1] Eterigho-Ikelegbe, Orevaoghene, et al., Materials Today: Proceedings, vol. 38, Elsevier BV, 2021, pp. 675-81. Crossref; https://doi.org/10.1016/j.matpr.2020.03.693

[2] Sobhani, Azam, MasoudSalavati-Niasari, Advances in Colloid and Interface Science, vol. 287, Elsevier BV, Jan. 2021, p. 102321. Crossref; https://doi.org/10.1016/j.cis.2020.102321

[3] Li, Binjie et al., Photonics and Nanostructures - Fundamentals and Applications, vol. 55, Elsevier BV, July 2023, p. 101151. Crossref; https://doi.org/10.1016/j.photonics.2023.101151

[4] Wang, Chanchan et al., Molecules, vol. 29, no. 5, MDPI AG, Feb. 2024, p. 1027. Crossref; https://doi.org/10.3390/molecules29051027

[5] Dong, Leyuan et al., Materials, vol. 17, no. 4, MDPI AG, Feb. 2024, p. 828. Crossref; https://doi.org/10.3390/ma17040828

[6] Safakas, Alexandros et al., Catalysts, vol. 13, no. 10, MDPI AG, Oct. 2023, p. 1342. Crossref; https://doi.org/10.3390/catal13101342

[7] Tsai, Wen-Tien, Atmosphere, vol. 14, no. 2, MDPI AG, Jan. 2023, p. 242. Crossref; https://doi.org/10.3390/atmos14020242

[8] Mistri, Rajib et al., Asian Journal of Chemistry, vol. 35, no. 11, Asian Journal of Chemistry, Oct. 2023, pp. 2631-39. Crossref; https://doi.org/10.14233/ajchem.2023.30271

[9] Rashidi, Rajab et al., Journal of Air Pollution and Health, Knowledge E, Feb. 2022. Crossref; https://doi.org/10.18502/japh.v6i4.8585

[10] Chen, Shuoqiu et al., Polymers, vol. 14, no. 17, MDPI AG, Aug. 2022, p. 3459. Crossref; https://doi.org/10.3390/polym14173459

[11] Bertheau, Elise, et al., Applied Sciences, vol. 14, no. 3, MDPI AG, Feb. 2024, p. 1266. Crossref; https://doi.org/10.3390/app14031266

[12] Zulhadjri, Zulhadjri et al., Materials Research, vol. 23, no. 2, FapUNIFESP (SciELO), 2020. Crossref; https://doi.org/10.1590/1980-5373-mr-2019-0521

[13] Zhang, Z., M. Greenblatt, Journal of Solid State Chemistry, vol. 111, no. 1, Elsevier BV, July 1994, pp. 141-46. Crossref; https://doi.org/10.1006/jssc.1994.1209

[14] Balch, Alan L., Krzysztof Winkler, Coordination Chemistry Reviews, vol. 438, Elsevier BV, July 2021, p. 213623. Crossref; https://doi.org/10.1016/j.ccr.2020.213623

[15] Gao, Yibo et al., Applied Catalysis B: Environmental, vol. 341, Elsevier BV, Feb. 2024, p. 123348. Crossref; https://doi.org/10.1016/j.apcatb.2023.123348

[16] Cheng, Xiaojing et al., Ceramics International, vol. 40, no. 4, Elsevier BV, May 2014, pp. 5771-79. Crossref; https://doi.org/10.1016/j.ceramint.2013.11.016

[17] Mantri, Sukriti, John E. Daniels, IEEE Transactions on Ultrasonics, Ferroelectrics, and Frequency Control, vol. 65, no. 9, Institute of Electrical and Electronics Engineers (IEEE), Sept. 2018, pp. 1517-24. Crossref; https://doi.org/10.1109/TUFFC.2018.2827406

[18] Xue, Dezhen et al., EPL (Europhysics Letters), vol. 100, no. 1, IOP Publishing, Oct. 2012, p. 17010. Crossref; https://doi.org/10.1209/0295-5075/100/17010

[19] Martínez, C. et al., Surface and Interface Analysis, vol. 34, no. 1, Wiley, Aug. 2002, pp. 524-26. Crossref; https://doi.org/10.1002/sia.1352

[20] Lee, Seungju, Daniel F. Shantz, Chemical Communications, no. 6, Royal Society of Chemistry (RSC), 2004, p. 680. Crossref; https://doi.org/10.1039/b315646j

[21] Merdrignac-Conanec, Odile, Patrick T. Moseley, " Journal of Materials Chemistry, vol. 12, no. 6, Royal Society of Chemistry (RSC), Apr. 2002, pp. 1779-81. Crossref; https://doi.org/10.1039/b111118n

[22] Oh, Seok-Young, Thi-HaiAnh Nguyen, Journal of Environmental Chemical Engineering, vol. 10, no. 2, Elsevier BV, Apr. 2022, p. 107386. Crossref; https://doi.org/10.1016/j.jece.2022.107386

[23] Torii, Hajime, Vibrational Spectroscopy, vol. 24, no. 1, Elsevier BV, Sept. 2000, pp. 3-14. Crossref; https://doi.org/10.1016/S0924-2031(00)00075-8

[24] Qi, Dabin, et al., Chemical Papers, vol. 76, no. 11, Springer Science and Business Media LLC, July 2022, pp. 6975-83. Crossref; https://doi.org/10.1007/s11696-022-02341-7

[25] Venkataswamy, Perala et al., Applied Surface Science, vol. 349, Elsevier BV, Sept. 2015, pp. 299-309. Crossref; https://doi.org/10.1016/j.apsusc.2015.04.220

[26] Vasilyeva, M. S. et al., Surface and Coatings Technology, vol. 275, Elsevier BV, Aug. 2015, pp. 84-89. Crossref; https://doi.org/10.1016/j.surfcoat.2015.05.035